2014 International Joint Conference on Neural Networks (IJCNN)
July 6-11, 2014, Beijing, China

Mimicking the worm – an adaptive spiking neural circuit for contour tracking inspired by *C. Elegans* thermotaxis

Ashish Bora
Department of Electrical Engineering,
Indian Institute of Technology, Bombay
Maharashtra, India 400076.
Email: ashish.dilip.bora@gmail.com

Arjun Rao
Department of Electrical Engineering,
Indian Institute of Technology, Bombay
Maharashtra, India 400076.
Email: arjun210493@gmail.com

Bipin Rajendran
Department of Electrical Engineering,
Indian Institute of Technology, Bombay
Maharashtra, India 400076.
Email: bipin@ee.iitb.ac.in

***Abstract*—We demonstrate a spiking neural circuit with timing-dependent adaptive synapses to track contours in a two-dimensional plane. Our model is inspired by the architecture of the $7-$neuron network believed to control the thermotaxis behavior in the nematode *Caenorhabditis Elegans*. However, unlike the *C. Elegans* network, our sensory neuron only uses the local variable (and not its derivative) to implement contour tracking, thereby minimizing the complexity of implementation. We employ spike timing based adaptation and plasticity rules to design micro-circuits for gradient detection and tracking. Simulations show that our bio-mimetic neural circuit can identify isotherms with a $\sim 60\%$ higher probability than the theoretically optimal memoryless Lévy foraging model. Further, once the set-point is identified, our model's tracking accuracy is in the range of $\pm 0.05\,^{\circ}$C, similar to that observed in nature. The neurons in our circuit spike at sparse biological rates (~ 100 Hz), enabling energy-efficient implementations.**

I. Introduction

Microbes and small organisms have been found to preferentially migrate along regions of identical temperature (thermotaxis) [1] or chemical concentration (chemotaxis) [2]. Such behavior is extremely important for the organism as it helps it to scavenge for food or to avoid noxious environmental conditions. In single-celled microbes, it is believed that such behaviors are mediated by chemoreceptor proteins which control the probability of tumbling resulting in a random walk that is biased towards the desired concentration or temperature. In higher organisms, it has been shown that there are specific sensory neurons and neural networks that control the run and turn probability, which in turn helps the organism to track contours of identical temperature or chemical concentration.

The nematode *Caenorhabditis Elegans* is widely considered today as the model organism for fundamental studies in developmental biology. Starting from the pioneering work of Sydney Brenner in the late 60s, significant progress has been made to identify the complete cell lineage, map the genome and also determine how higher level behavior emerges from the connectivity and function of neural networks. Among the many interesting behaviors exhibited by the nematode is its ability to track regions with constant temperatures or chemical concentrations. Hedgecock and Russell, in their seminal work in 1975 [3] showed that *C. Elegans* migrates to regions with temperature close to their cultivation temperature (T_c), and deviating from a given isotherm by as little as $0.05\,^{\circ}$C. Since then multiple experiments based on genetic mutations to alter individual cell responses and laser ablation studies to selectively infer the cells' role in controlling the overall behavior has helped throw light on the overall structure of the underlying networks that control these behaviors.

The contributions and organization of this paper is as follows. We develop a spiking neural circuit to track contours of physical environmental conditions such as temperature, chemical concentration of molecules etc. Our circuit is inspired by the biological neural networks underlying the thermotaxis behavior of *C. Elegans* (section II). However, unlike the *C. Elegans* network, the sensory neuron in our network only uses the local variable (and not its derivative) to implement contour tracking, thereby minimizing its complexity. We discuss the mathematical models for spiking neurons and synapses that we employ in section III. The algorithm we use for contour discovery and tracking is explained in section IV. The neural micro-circuits necessary for implementing this algorithm are developed in sections V and VI. We employ spike timing based adaptation and plasticity rules to implement gradient detection and tracking in our network. We study the performance of the network for various environmental profiles (section VIII) and propose methods for temporal and spatial scaling (section IX). We compare its performance with theoretically optimal foraging strategies and demonstrate the energy efficiency of our model based on the sparsity of spikes (section X).

II. *C. Elegans* thermotaxis network

A nearly complete structure and connectivity of the neural network of *C. Elegans* has been known for two decades [5]. There are 302 neurons in the adult organism, which are connected to each other through a network of ~ 5000 chemical synapses and 600 gap junctions. However, it is only recently that the functional connections in the network have begun to be elucidated to explain the origin of non-trivial behaviors such as thermotaxis from basic neural networks.

978-1-4799-1484-5/14/$31.00 ©2014 IEEE

Figure 1 shows a schematic of the neural network model believed to modulate the thermotaxis behavior in the worm. Temperature is sensed by AFD and AWC sensory neurons, which send signals of opposite polarity to the interneuron AIY. AIY synapses to interneurons AIZ and RIA and finally to motor neuron RIM which is believed to control the dynamics of locomotion of the worm to track isothermal regions [7]. It is believed that the worm executes thermotaxis by performing a biased random walk by switching between periods of long forward movements called 'runs' and sudden switches in directions called 'pirouettes'. It is found that as the worm approaches the desired temperature, the frequency of pirouettes decreases and run length increases. The opposite is true when the worm deviates from desired temperatures. Thus, a competition between these two strategies biases the worm towards desirable environmental conditions.

Experimental studies based on imaging of Ca^{2+} dynamics of cells, femto-second laser ablation and genetic mutations have been conducted to determine the cellular basis for thermotactic behavior [8]. When the local sensed temperature T is greater than the cultivation temperature T_c, the AFD neuron is activated, which in turn inhibits AIY. This suppresses the inactivation of AIZ neuron, causing the worm to move to lower temperatures (cryophilic behavior). On the other hand, when the local sensed temperature T is lesser than the cultivation temperature T_c, the AWC neuron stimulates AIY, promoting motion to warmer temperatures.

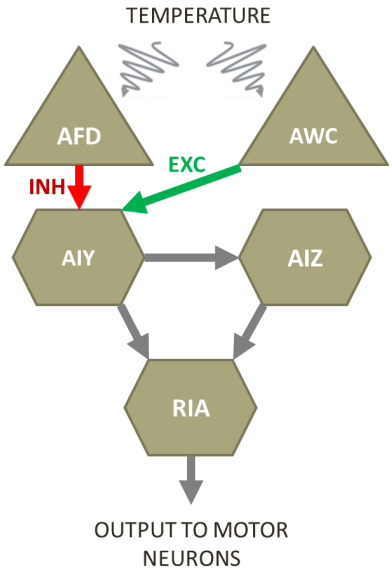

Fig. 1. Proposed model for thermotaxis network of *C. Elegans*, adapted from [4]. AFD and AWC sense the local temperature, and send signals of opposite polarity to the interneuron AIY which then propagates to interneurons AIZ, RIA and RIB and the motor neuron RIM (not shown).

III. Spiking Neural Network Implementation

Though there have been mathematical models to describe how thermotaxis arises due to the competitive behavior between cryophilic and thermophilic tracking [9], there have been no neural models that completely and quantitatively explain such behaviors. This is mainly due to the fact that no consistent picture exists for the cellular signaling schemes of all individual neurons believed to participate in tracking. In this paper, we look to the *C. Elegans* thermotaxis network for inspiration to design the basic architecture of a neural circuit for contour tracking. However, we have assumed that the neurons in our network perform integrate and fire dynamics and synaptic currents flow only in response to spikes, unlike some of the *C. Elegans* neurons which are known to issue plateau potentials [6]. Compared to the second generation artificial neural networks, spiking neural networks are believed to be more computationally efficient as larger fan-out circuits are possible and computations can be performed using spike times as the only token of information. The communication pathways in such networks are determined by the strengths of synapses, and hence a big challenge in designing such networks is to determine synaptic weights based on spike timing alone. In this paper, we develop biologically inspired models for synaptic plasticity to design various modules for our network.

We employ the following adaptive exponential integrate and fire (AEIF) model for modeling the dynamics of the neurons, with the parameters chosen to mimic the Regular Spiking (RS) neurons [10].

$$C\frac{dV(t)}{dt} = -g_L(V(t)-E_L) + g_L\Delta_T \exp\left(\frac{V(t)-V_T}{\Delta_T}\right) - U(t) + I_{app}(t) + I_{syn}(t) \quad (1)$$

$$\tau_w \frac{dU(t)}{dt} = a\left[V(t)-E_L\right] - U(t) \quad (2)$$

When $V(t) \geq 0$, $V(t) \longrightarrow V_r$ and $U(t) \longrightarrow U(t)+b$.

Synaptic currents due to a spike at time t^f is given by

$$I_{syn}(t) = I_s\left[\exp\left(-\frac{t-t^f}{\tau_m}\right) - \exp\left(-\frac{t-t^f}{\tau_s}\right)\right] h(t-t^f) \quad (3)$$

The values of the parameters used are listed in Table I.

IV. The Dynamics Model

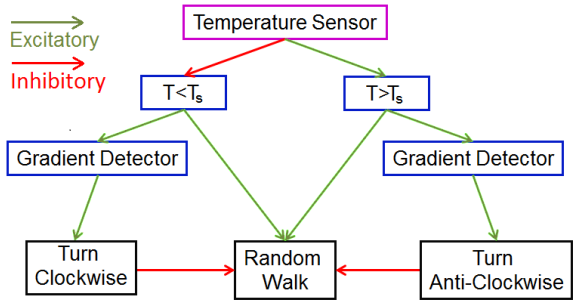

Fig. 2. Block diagram for the bio-inspired neural circuit for contour tracking. The model steers the worm to regions close to the set point T_s by controlling the probability for random walk and deterministic turns.

We now describe the salient aspects of the model to control locomotion for contour tracking by our artificial software 'worm'. If the worm is not near the desired set-point (T_s), it should exhibit random exploratory motion. The exploration should favor motion towards the directions in which the current local temperature (T) is more favorable

(small values of $|T - T_s|$) and shy away from directions of harsher temperature differences (large values of $|T - T_s|$). In this phase, worm should move rapidly so that a large area is quickly explored. On approaching the set-point, the tendency to execute random motion should decrease to enable tracking of the set-point isotherm. It is also desirable that the speed of the worm depends on $|T - T_s|$. When $|T - T_s|$ is large, larger speeds allow quick exploration of the space, while slower speeds are better near the isotherm to prevent overshooting or high amplitude oscillations during tracking.

The tracking model is inspired by the operation of AFD and AWC neurons of *C. Elegans* [8], [11]. However, unlike two or more temperature sensors present in the thermotaxis network of *C. Elegans*, our model employs one simple linear temperature sensor neuron. The tracking model is as follows. If the instantaneous temperature T is greater than the set-point T_s, and if the worm is encountering a positive gradient $(dT/dx > 0)$, we should alter the direction of motion. This is also true if the local temperature T is less than T_s, and the worm is encountering a negative gradient. We assume that in the former case, the worm turns clockwise and it turns anti-clockwise when the latter condition is satisfied. The choice of clockwise and anti-clockwise preference for turning is completely arbitrary. Further, making these opposing choices for turning instead of executing either clockwise or anti-clockwise turning for both the above mentioned conditions ensures that the worm does not go around in circles once it is in the vicinity of T_s. We will show that this tracking model employed in conjunction with random exploration can enable the worm to quickly identify the isotherms on a plane and to track it effectively.

In our model, the worm is continuously moving, and hence, the sign of gradient of temperature along the direction of worm movement is same as that of the temporal derivative dT/dt where t stands for time. Hence, we will use a temporal gradient detector instead of a spatial gradient detector for implementing our model. To summarize, we require the following basic blocks based on spiking neural networks to build our model:

1) Comparators to check $T > T_s$ or $T < T_s$
2) Gradient detectors to detect $dT/dt \gtrless 0$
3) A mechanism to control speed of the worm
4) A mechanism to introduce randomized exploration

In the following sections we show how these blocks can be built using neural circuits and subsequently combine them to form a contour tracker.

V. Micro-circuit for comparator

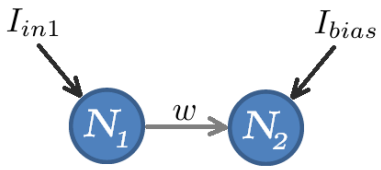

Fig. 3. Comparator neural circuit whose output spike frequency (at N_2) exhibits a linear dependence on ambient temperature T. N_1 is the sensory neuron, whose input current I_{in1} is linearly proportional to T. Parameters w and I_{bias} can be used to tune the response curve of the circuit.

We assume a simple model for the temperature sensor neuron, whose input current depends linearly on the local instantaneous temperature T. Based on the current-spike frequency characteristics of the AEIF spiking neuron, we assume the following temperature dependence, so that the spike frequency of the sensory neuron varies between $\sim 120\,\text{Hz}$ to $\sim 140\,\text{Hz}$ for a $\pm 0.05\,^\circ\text{C}$ variation around the temperature set point, T_s.

$$I_{in1} = \alpha_T + \beta_T \times (T - T_s) \tag{4}$$

where $\alpha_T = 600\,\text{pA}$ and $\beta_T = 500\,\text{pA/K}$. For the sake of explanation, we assume that the 'worm' is required to track a certain temperature, but in general, it could seek and track any other physical variable as long as the input sensor neuron has a similar linear dependence on that variable.

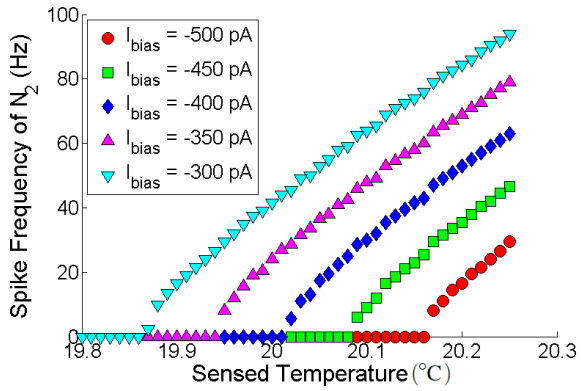

Fig. 4. Spike Frequency response of the comparator circuit (measured at N_2) for different values of I_{bias} (and a fixed value of $w = 205$). The threshold for detection can be tuned by varying the parameter I_{bias}.

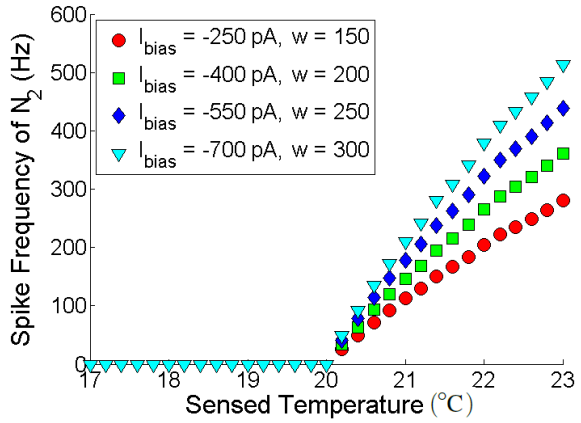

Fig. 5. The slope of the spike frequency response curve of the comparator circuit can be tuned by adjusting both the parameters I_{bias} and w.

The comparator consists of two neurons as shown in Figure 3. The spike frequency of N_2, determined by the bias current I_{bias} and the weight w of synapse $N_1 \rightarrow N_2$, shows a ramp-like output response (Figure 4, 5). Further, it is also possible to change the threshold for temperature detection, as well as the slope of the response independent of each other, by appropriately choosing the values for I_{bias} and w. A complementary comparator (i.e., a network that produces a proportional spike response for deviations of local temperature below the set-point) can be realized by making w negative and I_{bias} positive.

VI. Micro-circuit for gradient detector

A. Design and working principle

The gradient detector consists of three neurons N_4, N_5 and N_6 interacting through a network of four synapses with weights w_{45}, w_{46}, w_{56}, w_{66} (Figure 6). The input to the network is an analog current, I_{in} at neuron N_4, and N_6 is the output neuron. N_6 spikes when the network detects a positive gradient (w.r.t time) at the input current I_{in}. The synapse w_{46} is chosen to be excitatory, while w_{45} and w_{56} are inhibitory. Signal propagation through $N_4 \rightarrow N_5 \rightarrow N_6$ takes longer than through the direct path $N_4 \rightarrow N_6$. Since the currents in these paths have opposite signs, the effective spike frequency of N_6 should mimic a derivative operation.

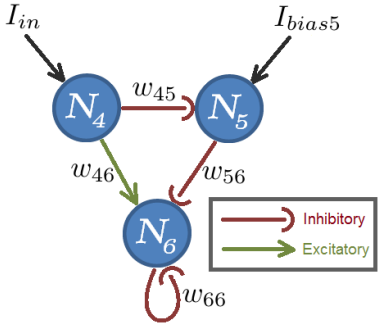

Fig. 6. The neural micro-circuit for gradient detection. N_6 spikes in response to positive gradients in the input current I_{in} at N_4. Synapses w_{45} and w_{56} are inhibitory, while w_{46} is excitatory. The strength of w_{56} depends on the time of arrival of spikes at N_5.

If I_{in} is constant for a sufficiently 'long' period of time, it is expected that N_6 should not spike. This can be achieved effectively if the strength of at-least one of the synapses in the network has a mechanism to adapt to the instantaneous value of I_{in}. Our model assumes that synaptic strength w_{56} adapts according the magnitude of I_{in}.

We denote the value of w_{56} for which the spiking of N_6 just stops as w_0. A small increase in w_{56} from this value will cause the N_6 to undergo periodic spiking. When $w_{56} = w_0$, there is an equilibrium between w_{46} injecting positive current into N_6 and $w_{56} = w_0$ opposing it. A weight adaptation rule that continuously pushes w_{56} towards w_0 is

$$\tau_a \frac{dw_{56}}{dt} = w_0 - w_{56} \tag{5}$$

w_0 is not a constant, but a monotonically decreasing function of the input current. The above equation ensures that when I_{in} is constant, w_{56} converges to w_0, prohibiting N_6 from spiking. When I_{in} increases, the equilibrium is disturbed such that spike rate of N_4 is increased and spike rate of N_5 is decreased due to increase in inhibiting current induced by w_{45}. Thus, N_6 sees an increase in the incoming positive current through w_{46} and a decrease in inhibition through w_{56}. The net excitatory current coming into N_6 thus increases, causing it to spike. N_6 continues to spike until the weight w_{56} converges (as per (5)) to the value of w_0 corresponding to the new I_{in}. This process of adaptation is not instantaneous allowing for sufficient spiking at N_6.

When I_{in} decreases, excitatory current to N_6 through w_{46} decreases. In addition, spiking of N_5 increases which increases inhibitory current through w_{56}. Thus through both w_{46} and w_{56}, spiking of N_6 is suppressed. w_{56} then increases to reach the now less negative w_0, always staying below it, thus continuously suppressing spiking of N_6.

B. Determining the parameters of the adaptation rule

To begin with, the weights w_{46} is chosen to be 200 while w_{45} is chosen to be -50; the initial value of w_{56} is immaterial, as the weight adaptation rules changes it according to the spiking frequency of N_5 (denoted by f_5). The chosen parameters in our design ensures that gradients are detected when the input current (I_{in}) lies between 600 pA to 1100 pA. Figure 7 shows w_0, the maximum (least negative) value of weight w_{56} which results in no spiking at the output neuron N_6 for different values of I_{in}, as a function of the spike rate f_5 of neuron N_5.

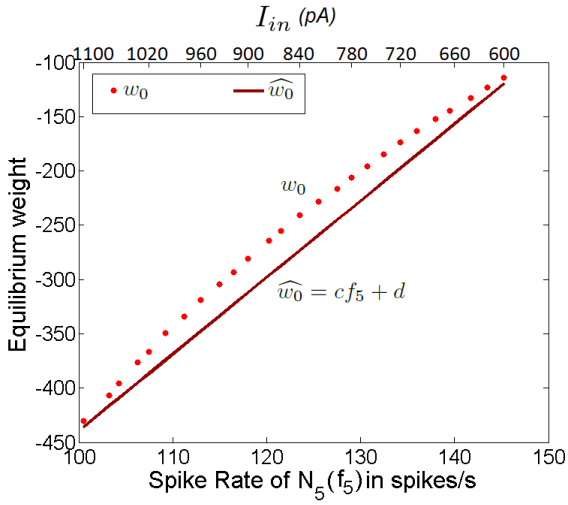

Fig. 7. The critical value w_0 of strength of synapse w_{56} for which the gradient detector stops responding as a function of the spike rate of N_5. The linear approximation $\widehat{w_0}$ is used to develop the adaptation rule for the synapse w_{56} of the gradient detector circuit.

w_0 has a non-linear dependence on f_5, but to minimize the complexity of implementation, we use the following linear rule, given by

$$\widehat{w_0} = cf_5 + d \tag{6}$$

Note that $\widehat{w_0}$ is not a least square approximation for the $w_0 - f_5$ dependence, and is intentionally chosen such that in the given operating range, $\widehat{w_0} < w_0$. The operating range for the input current and the corresponding parameters for $\widehat{w_0}$ are chosen such that the relative error of $\widehat{w_0}$ w.r.t w_0 is small. For any value of I_{in}, if $\widehat{w_0} > w_0$, then w_{56} would converge to a value greater than the maximum value that would suppress the spiking of N_6, leading to unnecessary spikes in the output neuron. If $\widehat{w_0}$ is significantly smaller than w_0, this would lead to loss of sensitivity of the gradient detector. For obtaining reasonable spiking at N_6, it would therefore be necessary for I_{in} to counter-act the additional inhibition by the overcompensated value of w_{56}.

It is obvious that recurrent spiking for any constant input current clearly violates the desired function of the gradient detector. We have decided to limit the sensitivity

of the gradient detector to 40 pA/s to ensure that there is no recurrent spiking in the chosen operating range of I_{in}. Combining equations 5 and 6, the adaptation rule becomes

$$\frac{dw_{56}}{dt} = \left(\frac{c}{\tau_a}\right) f_5 + \frac{(d - w_{56})}{\tau_a} \quad (7)$$

$$\Rightarrow \Delta w_{56} = \left(\frac{c}{\tau_a}\right) f_5 \Delta t + \frac{(d - w_{56})}{\tau_a} \Delta t \quad (8)$$

The above relationship requires the knowledge of the arrival rate of spikes in the recent past (to obtain f_5). In order to avoid this, and develop memoryless adaptation, we propose

$$\Delta w_{56} = \left(\frac{c}{\tau_a}\right) \delta(t - t^{N_5}) + \frac{(d - w_{56})}{\tau_a} \Delta t \quad (9)$$

where t^{N_5} denotes the instants where neuron N_5 has spiked.

The first term represents an increment in w_{56} triggered by every spike at N_5. The second term represents the natural tendency of the synapse to push its weight towards the value d. This modification allows us to adapt w_{56} based on spike occurrence at N_5 and current value of w_{56}. These are local variables for w_{56} and do not require any memory of the past [13]. It can be observed from Figure 8 that the proposed model performs the desired gradient detection operation.

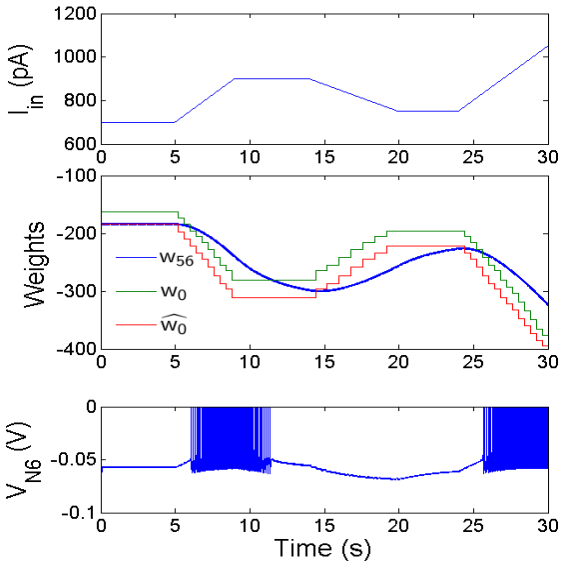

Fig. 8. Output of the gradient detector micro-circuit, showing the input current (top panel), weight adaptation (middle) and the spike response (bottom). N_6 spikes only when there is positive gradient in I_{in} and it stops spiking if and only if $w_{56} < w_0$. Notice that w_{56} continuously moves towards the steady state value $\widehat{w_0}$.

C. Customization, control and tradeoffs

We now discuss parameters in the network that can be used to customize key descriptors of the gradient detector such as sensitivity, noise tolerance and response time.

1) τ_a: This variable determines the rate at which adaptation of w_{56} occurs. Small values of τ_a lead to w_{56} reaching its new equilibrium before the neuron N_6 spikes a sufficient number of times. This would mean that N_6 spikes sufficiently only if I_{in} changes rapidly, reducing the sensitivity of the gradient detector. Such a circuit would also be susceptible to noise since large gradients are being detected in small time intervals. Large values of τ_a would result in sustained spikes in the output neuron even after the gradient at the input vanishes.

2) w_{46}: w_{46} controls the amplification of the difference between inputs from N_4 and N_5 into N_6. This is because of the fact that $|w_0|$ increases with w_{46}. A decrease in w_{46} would lead to loss in sensitivity and will increase response time. On the other hand, a large value would result in quick response (which worsens noise tolerance) and also lead to sustained spikes after the gradient has disappeared.

3) w_{66}: We add a self-inhibitory synapse w_{66} for the output neuron N_6 to selectively reduce the spike frequency at high gradients. This is necessary to avoid the worm moving in circles in regions of high gradients.

VII. Neural Circuit for Contour Tracking

In this section, we proceed to combine the comparator and gradient detector circuits to make a non-favorable direction detector. We introduce a mechanism for random exploration and speed control model with their implementations in conjunction with non-favorable direction detector. We will show that this circuit is capable of exploring a region with varying temperatures and detect and track a desired set temperature. The complete combined circuit and the values of the bias currents and synaptic strengths used in the simulations is shown in Figure 9 and Table II.

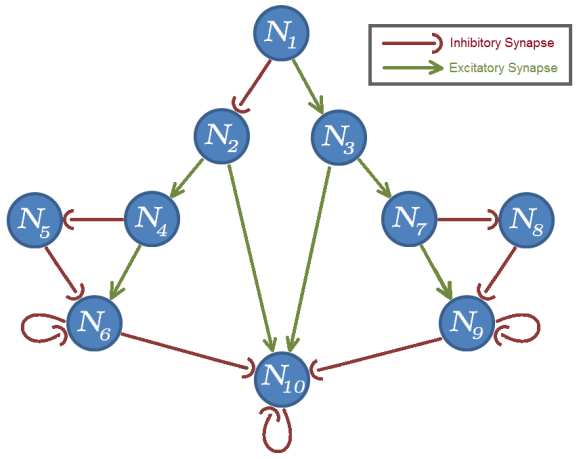

Fig. 9. Schematic of the neural circuit for contour tracking. N_1 is a temperature sensitive input neuron. $N_1 - N_3$ is a positive comparator, and $N_7 - N_8 - N_9$ is a gradient detector. Similarly, $N_1 - N_2$ is a complementary comparator, and $N_4 - N_5 - N_6$ is a gradient detector. N_6 and N_9 control the deterministic turns, while N_{10} controls the random exploration.

A. Non-favorable direction detection

N_1 is a linear temperature sensor neuron, whose temperature dependent input current is given according to equation 4, where $\alpha_T = 600$ pA and $\beta_T = 500$ pA/K. We have assumed $T_s = 20\,^{\circ}$C. By tuning the parameters of the model, it is possible to track other temperatures as shown in Figure 12.

TABLE I. PARAMETERS USED IN SIMULATION

Parameter	Value	Parameter	Value
C	200 pF	V_r	-58 mV
g_L	10 ms	b	0 pA
E_L	-70 mV	τ_m, τ_v	15 ms
Δ_T	2 mV	τ_s	3.75 ms
V_T	-50 mV	c	7.0614 Hz^{-1}
τ_w	30 ms	d	-1145.176
a	2 nS	τ_a	3 s

TABLE II. VALUES OF SYNAPTIC STRENGTHS AND BIAS CURRENTS FOR THE CIRCUIT TO TRACK $T_s = 20\,^\circ$C

Parameter	Value	Parameter	Value	Parameter	Value
w_{12}	-205	w_{13}	207	I_{bias2}	830.5 pA
w_{24}	120	w_{37}	100	I_{bias3}	-396 pA
w_{45}	-50	w_{78}	-50	I_{bias4}	600 pA
w_{46}	200	w_{79}	200	I_{bias5}	800 pA
$w_{6,10}$	-1000	$w_{9,10}$	-1000	I_{bias7}	600 pA
$w_{2,10}$	6.089	$w_{3,10}$	6.755	I_{bias8}	800 pA
w_{66}, w_{99}	-200	$w_{10,10}$	-800	I_{bias10}	205 pA

The network $N_1 - N_3$ is a positive comparator, that spikes only if $T > T_s$. Based on the comparator architecture described in section V, the synapse $N_1 \rightarrow N_3$ is excitatory and N_3 receives a negative bias current.

Neurons N_7, N_8 and N_9 together form a gradient detector. N_7 receives a constant bias current and N_3 feeds this gradient detector through the synapse $N_3 \rightarrow N_7$. For $T < T_s$, N_3 does not spike and hence, N_7 does not receive any input from N_3. Thus, there is no gradient at input current to N_7 and consequently, N_9 cannot spike. For $T > T_s$, response of N_3 linearly increases with sensed temperature (Figures 4, 5). Thus increase in T results in a gradient at input current to N_7, which is detected by the gradient detector. Therefore, spiking at N_9 is indicative of $T > T_s$ and $dT/dt > 0$. As per the motion model, at every spike of N_9, the worm turns by 7.5° in anticlockwise direction.

In an exactly parallel fashion, the network $N_1 - N_3$ is a complementary comparator, that spikes only if $T < T_s$. Synapse $N_1 \rightarrow N_2$ is inhibitory and N_2 receives a positive bias current. Neurons N_4, N_5 and N_6 together form another gradient detector. N_2 feeds this gradient detector through the synapse $N_2 \rightarrow N_4$ and by similar logic, spiking at N_6 indicates $T < T_s$ and $dT/dt < 0$. At every spike of N_6, the worm turns by 7.5° in clockwise direction.

B. Random exploration model and implementation

We introduce neuron N_{10} to actuate the random exploratory motion in the plane by the worm. We achieve this by stipulating that at every spike of N_{10}, the worm turns by a random angle uniformly distributed over $-\pi/2$ to $+\pi/2$. As described in Section IV, it is necessary that this neuron spikes only when the worm is not near T_s. To ensure this, the bias current into N_{10} is chosen such that it alone is not sufficient to elicit any spiking in N_{10}. The two comparator circuits are designed such that at least one of the neurons N_2 and N_3 spike heavily if the worm is not near T_s. Synapses $N_2 \rightarrow N_{10}$ and $N_3 \rightarrow N_{10}$ inject excitatory currents, so that N_{10} spikes when worm is not within a band around the cultivation temperature T_s.

During random exploration, it is desirable to have sufficient run lengths. This can be possible if the spiking of N_{10} is made sparse. This is ensured by two means. Firstly, synapses $N_2 \rightarrow N_{10}$ and $N_3 \rightarrow N_{10}$ are given small weights. Thus the run length is a slowly decreasing function of $|T - T_s|$. Secondly, a self-inhibiting loop is added at N_{10} to further increase the run length. If the worm is facing towards a non-favorable direction, it is most important to turn away from such directions. Thus, in such cases randomness should be suppressed. Since spiking at either N_6 or N_9 is indicative of non-favorable directions, inhibitory synapses $N_6 \rightarrow N_{10}$ and $N_9 \rightarrow N_{10}$ are added.

C. Speed control

As described in Section IV, the worm should move faster if it is away from T_s. To achieve this, we stipulate that for every spike of either N_2 or N_3, the magnitude of the speed is incremented by a constant amount (1.3 mm/sec). In absence of any spike at either N_2 or N_3, the speed exponentially decays to 1 mm/sec with a time constant τ_v.

To summarize, our model consists of 10 neurons. It has one linear temperature sensor, two neurons that together influence the speed of the worm and three neurons that control turning. Two of the turning control neurons actuate deterministic clockwise and anticlockwise turning, while the third one actuates random turning.

VIII. SIMULATION RESULTS

Figure 10 shows a typical motion profile executed by our worm for a set-point of $T_s = 20\,^\circ$C. Initially, the worm executes random exploratory motion till it comes to the vicinity of T_s and then tracks the isotherm, with standard deviation around the isotherm maintained at $\sim 0.05\,^\circ$C. The spike patterns in the network during random motion and tracking is shown in Figure 11. By altering the parameters of comparators, it is also possible to change the set-point, and make the model track other temperatures. Figure 12 (Trajectory 1) shows the profile of a worm launched from the same initial point as in Figure 10, but with $T_s = 18.6\,^\circ$C. Trajectory 2 in figure 12 shows that the worm is able to identify and track the isotherm even if the launch point is at a temperature that is higher than the set-point of $T_s = 20\,^\circ$C.

We also show that our model performs exploration and tracking exceptionally well even in noisy environments. Figure 13 show the exploration trajectory traced by the worm launched from the same point in the plane, but with noise added to the background temperature profile.

IX. SCALING

In this section, we discuss the principles for scaling our model's tracking behavior to operate in different spatial or temporal ranges. For the circuit to function as desired, it is necessary that the input currents to the gradient detectors, i.e input to N_4 (I_{in4}) and N_7 (I_{in7}) remain within the operating range of the gradient detectors and the time derivatives of these currents be maintained. Since comparators $N_1 - N_2$ and $N_1 - N_3$ have ramp responses (refer Figure 5), the input

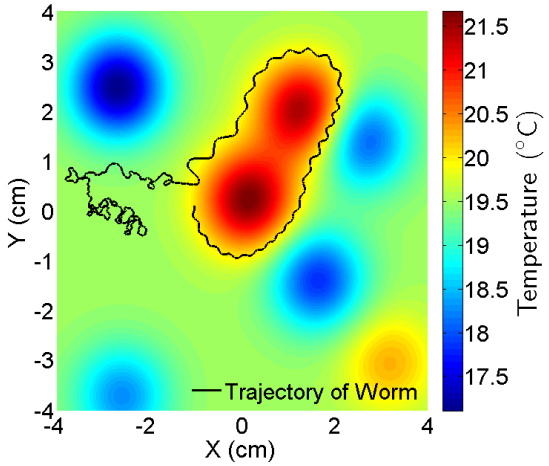

Fig. 10. Trajectory of the worm which starts at a low (undetectable) gradient region and reaches and tracks the set-point temperature (T_s = 20 °C) through random motion.

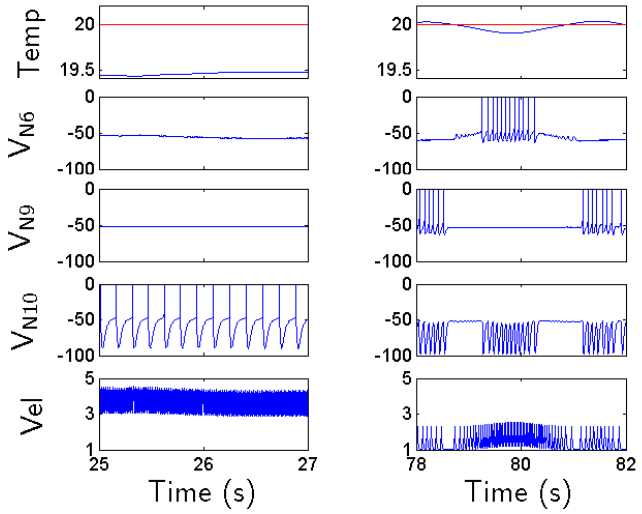

Fig. 11. Spike patterns in the network during random exploration (left) and tracking (right). N_6 and N_9 spike in response to negative and positive temperature gradients. Their spikes actuate deterministic turns causing isothermal tracking. N_{10} spikes when they are quiet, prompting random exploration. Also, when away from T_s heavy spiking at comparator neurons causes the average speed to increase thus leading to faster coverage of the space. (Temp is in °C, Neuron voltages in mV and Vel in mm/s).

currents to the gradient detectors are linear functions of I_{in1} in their respective operating ranges. Hence,

$$\frac{dI_{in4}}{dt} = \frac{d}{dt}\left(I_{bias4} + I_{24}\right) = \frac{dI_{24}}{dt} \propto \frac{dI_{in1}}{dt} \tag{10}$$

If we denote the spatial variable in the direction of movement of the worm by r, then Equation 4 implies

$$\frac{dI_{in1}}{dt} = \left(\frac{dI_{in1}}{dT}\right)\left(\frac{dT}{dr}\right)\left(\frac{dr}{dt}\right) = \beta_T \frac{dT}{dr} v \tag{11}$$

Thus, for a given spatial (dT/dx) or temporal (v) scaling, β_T can be adjusted so that dI_{in4}/dt (and dI_{in7}/dt) remain same. However, β_T should not be very high to maintain the operating range of gradient detectors. The weights $w_{2,10}$ and

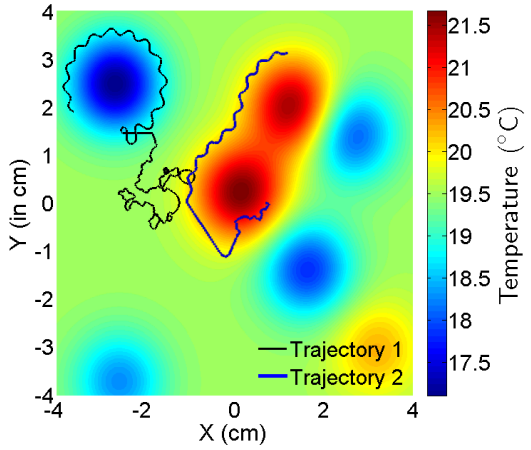

Fig. 12. Trajectory 1 shows the worm tracking a new temperature as a result of changing the T_s parameter to 18.6 °C in Equation (4). In Trajectory 2, the worm starts at a temperature higher than T_s = 20 °C.

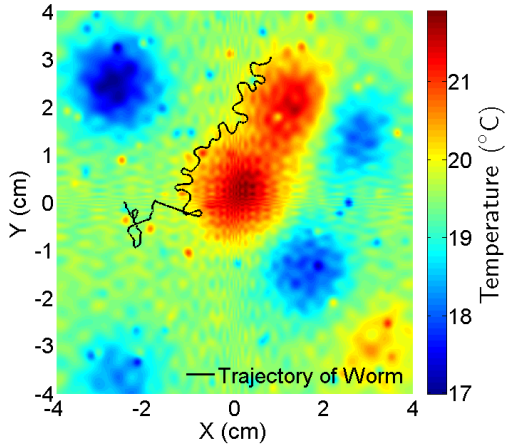

Fig. 13. Performance of the worm in presence of additive salt and pepper noise (sprinkled with a density of $100/64\,\text{cm}^2$). The noise has high harmonic amplitude in the frequency range of $3\,\text{cm}^{-1}$ to $10\,\text{cm}^{-1}$ and mean square amplitude of 0.1558 °C.

$w_{3,10}$ must be adjusted for the new values of β_T, so that N_{10} spikes only outside a required band of temperatures.

X. Performance Evaluation

To quantify the foraging ability of our model, we measured the average time taken by the worm to reach the isotherm (T_s = 20 °C) over repeated experiments, when launched from the same location. Of the 200 simulations performed, our model identified and tracked the isotherm in $\sim$ 63% cases within 150 s. Further, the time to locate the isotherm was $40.70\,\text{s} \pm 27.83\,\text{s}$. Once the worm settles into the tracking mode, its path lies on a band around the isotherm $0.03 - 0.09$ °C wide, with an average deviation of 0.05 °C.

It is well-known that the optimal strategy to detect randomly distributed targets is to make the flight lengths between random turns follow the heavy-tailed Lévy distribution [12]. We simulated this strategy by drawing the

run-lengths l from a truncated heavy tailed distribution (whose p.d.f is $P(l) \sim l^{-2}$ in the interval of $[s, 20s]$ where $s = 0.51\,\text{mm}$ is the empirically determined minimum run length of the neural model). The isotherm was reached in only $\sim 39\%$ of the experiments and the average time for detection increased to $51.08\,\text{s}$ $\pm 36.16\,\text{s}$ with the same foraging velocity as the neural model. Success criteria for foraging is set as the flight path encountering a band of $\pm 0.05\,^{\circ}\text{C}$ around T_s.

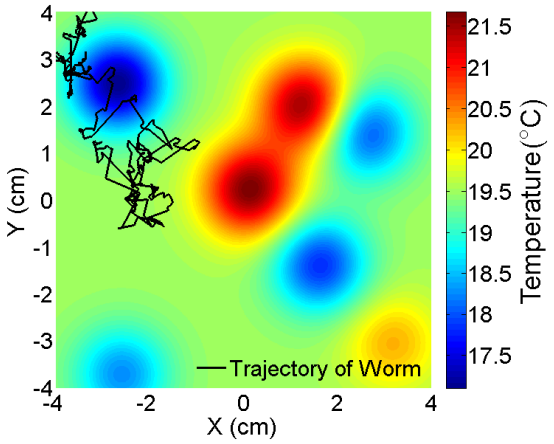

Fig. 14. Unlike our neural model, Lévy foraging fails to use local information to steer the worm away from unfavorable directions. A typical Lévy flight track launched from the same location as before, which failed to detect the set point ($T_s = 20\,^{\circ}\text{C}$) within $150\,\text{s}$ is shown.

It is clear that the network we developed for our model outperforms the Lévy flight strategy, both in terms of the mean time for success and its reliability measured in terms of its variance. Unlike our model, the Lévy flight strategy does not steer the worm away from unfavorable directions during exploration, making its overall performance inferior to our model (Figure 14). This clearly demonstrates that the energy expended by the worm in doing complex computations is actually useful as it performs better than an optimal memoryless foraging strategy.

Further, we monitored the firing rates of the neurons in our model, as the energy consumed by a hardware implementation of this circuit will depend on the number of spikes needed to make decisions. The average firing rate (calculated over $150\,\text{s}$ duration) over the whole population of neurons is $73.89\,\text{Hz}$. Neurons 4, 5, 7 and 8 spike at $\sim 130\,\text{Hz}$ while other neurons spike rarely. In particular, the neurons 6, 9, 10 spike at $2\,\text{Hz}$ on average. The histogram of local spiking frequency calculated over a $500\,\text{ms}$ window peaks sharply near $0\,\text{Hz}$, indicating that the neurons spike sparsely. Local spiking frequencies rarely go above $150\,\text{Hz}$ and never above $260\,\text{Hz}$, ensuring that our model is biologically plausible.

XI. Conclusion

In this paper, we have developed a spiking neural circuit inspired by the thermotaxis network of the nematode *C. Elegans*. Our circuit, consisting of only 10 spiking neurons and one simple linear, local temperature sensor neuron, is able to explore, identify and track a programmable set-temperature to a high degree of accuracy.

We have shown that our model outperforms the theoretically optimal memoryless foraging strategy based on the Lévy distribution by $\sim 60\%$ in terms of the probability for finding the isotherm. Further, once the isotherm is determined, our model tracks the set-point with an accuracy of $\sim 0.05\,^{\circ}\text{C}$, which is similar to the accuracy seen in nature [3]. We have also demonstrated that that the model is robust in the presence of noise.

Our model is general enough to be modified to track other environmental variables such as chemical molecules, radiation, etc by choosing appropriate sensor neurons. By turning off the negative gradient detector, we can modify this model to seek the source of diffusive stimulants. With simple modifications, our model can also be used for navigation and obstacle avoidance. We have also shown that by appropriately modifying the sensitivity of the sensor neuron, our model can perform tracking in various spatial and temporal scales. The neurons in our network spike at sparse biological rates ($\sim 100\,\text{Hz}$), showing that complex computations can be performed in an energy-efficient manner.

Acknowledgment

We gratefully acknowledge valuable discussions with Dr. Mark Ritter and Dr. Seyoung Kim at IBM T. J. Watson Research Center and Sai Bhargav Yalamanchi and Akshat Kadam from IIT Bombay.

References

[1] K. L. Poff and M. Skokut, *Thermotaxis by pseudoplasmodia of Dictyostelium discoideum.* PNAS, 74: 2007-2010 (1977).

[2] J. Adler, W-W. Tso, *"Decision"-Making in Bacteria: Chemotactic response of Escherichia coli to conflicting stimuli* Science, 21 June 1974, Vol. 184, no. 4143, pp. 1292-1294.

[3] E. M. Hedgecock, R. L. Russell *Normal and mutant thermotaxis in the nematode Elegans*. Proc Natl Acad Sci USA, 72:4061-4065.

[4] N. Ohnishi, A. Kuhara, F. Nakamura, Y. Okochi, I. Mori *Bidirectional regulation of thermotaxis by glutamate transmissions in Caenorhabditis Elegans*. The EMBO Journal (2011) 30, 1376-1388.

[5] J. G. White, E. Southgate, J. N. Thomson and S. Brenner *The structure of the nervous system of Caenorhabditis Elegans.* Philos Trans R Soc Lond B Biol Sci 314: 1-340.

[6] J. E. Mellem, P. J. Brockie, D. M. Madsen, and A. V. Maricq, *Action Potentials Contribute to neuronal signaling in C. Elegans.* Nat Neurosci. 2008 August; 11(8): 865-867.

[7] J. M. Gray, J. J. Hill, and C. I. Bargmann, *A circuit for navigation in C. Elegans*, PNAS March 1, 2005 vol. 102 no. 9, 3184-3191.

[8] D. A. Clark, D. Biron, P. Sengupta, and A. D. T. Samuel, *The AFD sensory neurons encode multiple functions underlying thermotactic behavior in Caenorhabditis Elegans*, The Journal of Neuroscience, July 12, 2006, 26(28):7444-7451.

[9] T. Matsuoka, S. Gomi, R. Shingai, *Simulation of C. Elegans thermotactic behavior in a linear thermal gradient using a simple phenomenological motility model*, J. of Theor. Bio. 250, 230-43 (2008).

[10] R. Brette & W. Gerstner, *Adaptive Exponential I&F model as an effective description of neuronal activity*, J Neurophysiol 94, pp. 3637-3642 (2005).

[11] K. Kimura, A. Miyawaki, K. Matsumoto, I. Mori, *The C. Elegans thermosensory neuron AFD responds to warming*, Current Biology, Volume 14, Issue 14, 27 July 2004, Pages 1291-1295.

[12] G. M. Viswanathan, S. V. Buldyrev, S. Havlin, M. G. E. da Luz, E. P. Raposo and H. E. Stanley, *Optimizing the success of random searches*, Nature 401, 911-914 (28 October 1999).

[13] C. Soto-Trevino, K. A. Thoroughman, E. Marder, L. F. Abbott, *Activity-dependent modification of inhibitory synapses in models of rhythmic neural networks*, Nature Neurosci. 2001 Mar;4(3), 297-303.